Langmuir

Article

pubs.acs.org/Langmuir

Self-Assembled Monolayers of NH_2-Terminated Thiolates: Order, pK_a, and Specific Adsorption

Waldemar A. Marmisollé, Daiana A. Capdevila, Ezequiel de la Llave, Federico J. Williams, and Daniel H. Murgida*

Departamento de Química Inorgánica, Analítica y Química Física and INQUIMAE, Facultad de Ciencias Exactas y Naturales, Universidad de Buenos Aires and CONICET, Ciudad Universitaria, pab. 2, piso 3, C1428EHA-Buenos Aires, Argentina

Supporting Information

ABSTRACT: Self-assembled monolayers (SAMs) of amino-terminated alkanethiols on Au were characterized by a combination of electrochemical (LSV, CV, and EIS) and spectroscopic (XPS and SER) techniques. Clear correlations were obtained between the apparent surface pK_a values determined by impedimetric titrations and order parameters such as the content of trans conformers in the SAMs. These results contrast with previous studies that exhibit dispersions of up to 6 pH units in the reported pK_a values. In addition, we determined that inorganic and organic phosphate species bind specifically to these SAMs mediating adsorption and heterogeneous electron transfer of positively charged macromolecules such as cytochrome *c*.

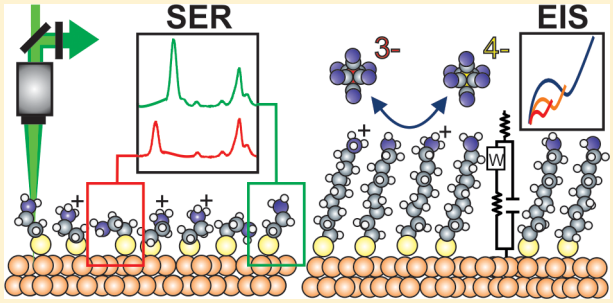

INTRODUCTION

Self-assembled monolayers (SAMs) of ω-functionalized alkanethiols represent a powerful and widespread approach for tailoring surface properties of coinage metals such as wettability, hydrophobicity, and charge density, which are of the utmost importance in defining their interaction capabilities. By proper selection or modification of the tail groups, SAMs provide tunable links between both macroscopic and nanometric metal structures with inorganic, organic, and biological materials, thus constituting key components for the rational design of complex arrays in the broad field of nanoscience and nanotechnology including applications such as plasmonics, nanoelectrochemistry, and molecular electronics, among others.[1] SAMs of thiolates also find a number of important applications in biology and biochemistry that include biosensing, characterization of interactions between biomolecules and cell-surface receptors, protein electron transfer, and others.[2−5] Due to their applicability, these coatings have been extensively characterized over the last decades by a variety of experimental and theoretical methods, and their properties and applications have also been comprehensibly reviewed.[1,6,7]

Amino-terminated SAMs constitute an interesting example of surface functionalization as they have been employed for various purposes such as promoting deposition of positive and negative inorganic films,[8,9] modulating interactions of biomaterials with surfaces, biocompatible incorporation of nanostructures into living cells,[10] assembly of DNA arrays,[11] and anchoring of carbon nanotubes and Au nanoparticles on electrodes for facilitating interfacial electron transfer (ET).[12−14] In spite of being broadly utilized, these SAMs have not been systematically characterized to the same level of detail as others. Indeed, information about their structure, stability, acid−base properties, specific adsorption of species, permeability, and applicability as spacers for heterogeneous ET is relatively scarce and often contradictory.[12,13,15−19] This knowledge, however, is essential for most applications as, for instance, the rational design of bio- and nanodevices. SAM order degree limits or regulates permeation and contact of the metal surface with the solution. The surface charge of the monolayers controls the electrostatic interactions with other materials such as nanoparticles, proteins, or living cells. This charge, in turn, is largely determined by the acid−base equilibrium of amino groups but may also be affected by specifically adsorbed ionic species. Poor control or understanding of these properties unavoidably leads to unclear results. A good example of this is the contradictory reports about immobilization and heterogeneous ET of the basic redox protein cytochrome *c* (Cyt) on SAMs of NH_2-terminated thiolates. Different authors have reported that (i) Cyt is not able to absorb on cysteamine SAMs,[14] (ii) Cyt is able to adsorb on electrodes coated with NH_2-terminated SAMs but in an orientation that prevents direct electrochemistry,[20] and (iii) Cyt adsorbs on NH_2-terminated SAMs and exhibits good electrochemical response.[21] A more recent study demonstrated that Cyt is actually able to bind NH_2-terminated SAMs provided that inorganic or organic phosphate species are present in the incubation solution and that, in this case, the orientation of the adsorbed protein is optimized for efficient heterogeneous ET.[22]

Received: November 29, 2012
Revised: February 27, 2013
Published: April 7, 2013

   dx.doi.org/10.1021/la304730q | *Langmuir* 2013, 29, 5351−5359

Here we present a spectroscopic (XPS and SER) and electrochemical (LSV, CV, and EIS) characterization of SAMs of NH_2-terminated thiols. Specifically, we focus on SAM order, acid−base equilibrium, and affinity for inorganic and organic phosphate species as a function of the chain length of the alkanethiol and as a function of dilution with OH-terminated thiolates. In addition to this per se valuable information, the results provide sound basis for understanding the immobilization and ET dynamics of Cyt on this type of assemblies.

EXPERIMENTAL SECTION

Chemicals. Cysteamine hydrochloride (NH_2-C2), 6-mercapto-1-hexanol (OH-C6), 8-mercapto-1-octanol (OH-C8), 11-mercapto-1-undecanol (OH-C11) were purchased from Sigma-Aldrich. 6-Amino-1-hexanethiol hydrochloride (NH_2-C6), 8-amino-1-octanethiol hydrochloride (NH_2-C8), 11-amino-1-undecanethiol hydrochloride (NH_2-C11), and 16-amino-1-hexadecanethiol hydrochloride (NH_2-C16) were purchased from Dojindo. 16-Mercapto-1-hexadecanol (OH-C16) was purchased from Frontier Scientific. All were used without further purification.

All chemicals were of analytical grade. The water used in all experiments was purified by a Millipore system and its resistance was 18.2 MΩ.

X-ray Photoelectron Spectroscopy (XPS). XPS measurements were performed using an ultrahigh vacuum chamber (UHV; base pressure <5.10−10 mbar) with a SPECS UHV spectrometer system equipped with 150 mm mean radius hemispherical electron energy analyzer and a nine channeltron detector. The chamber is equipped with a transfer system built in our laboratory that allows easy and rapid controlled transfer of the sample between the UHV environment and the atmospheric liquid environment. Self-assembled monolayer formation was carried out on the liquid reactor interfaced with the main analysis UHV chamber. This experimental setup permits performing ex-situ electron spectroscopic measurements on samples that are initially clean in UHV and not exposed to the laboratory atmosphere. Therefore we have full spectroscopic knowledge of the initial state of the sample before monolayer formation. The Au crystal was Ar^+ sputtered (E = 1000 eV) and annealed (T = 625 K) in subsequent cycles until no impurities are detected by XPS (only Au related peaks are observe in the XPS spectra). The spectroscopically clean Au crystal is transferred from the UHV environment to the liquid environment without exposure to the laboratory atmosphere where the SAM is formed. Spectra were acquired at a constant pass energy of 20 eV using a unmonochromated MgKα (1253.6 eV) source operated at 12.5 kV and 20 mA and a detection angle of 30° with respect to the sample normal on grounded conducting substrates. Quoted binding energies are referred to the Au 4f7/2 emission at 84 eV. Atomic ratios were calculated from the integrated intensities of core levels after instrumental and photoionization cross section correction.

Surface-Enhanced Raman Spectroscopy. SER spectra were measured with cw excitation of an argon ion laser (514 nm, Coherent Innova 70C) using a confocal Raman microscope (Jobin Yvon HR800) equipped with a liquid-nitrogen cooled CCD detector. The laser beam was focused onto the surface of a rotating Ag electrode by means of a long-working-distance objective (20×, numerical aperture 0.35). The spectroelectrochemical cell for SER determinations has been described elsewhere[23] and was controlled with a Teq03 potentiostat. Experiments were performed with laser powers of ca. 12 mW at the sample.

Voltammetry and Electrochemical Impedance Spectroscopy. Linear sweep voltammetry (LSV), cyclic voltammetry (CV), and electrochemical impedance spectroscopy (EIS) experiments were performed using a Gamry REF600 potentiostat equipped with Vista Shield Faraday cage. As working electrodes we used polycrystalline Au beads. All electrode potentials cited in this work were measured against Ag/AgCl (3 M KCl) and the counter electrode was a platinum wire. Aqueous solutions were exhaustively deoxygenated by bubbling Ar previous to the measurements and Ar overpressure was maintained during the experiments. Measurements were carried out at room temperature (22−24 °C). Unless stated otherwise, electrolyte solutions were 0.01 M phosphate buffer of pH 7 (Pi).

Impedance spectra in the range 10^5−10^{-1} Hz were recorded with a 10 mV rms amplitude potential perturbation. 1 mM solutions of $K_4Fe(CN)_6$ and $K_3Fe(CN)_6$ and 0.1 mM solutions of $Ru(NH_3)_6Cl_3$ were prepared in each electrolyte from 10 mM stock solutions. For titration experiments, the pH of the solution was varied by mixing 1 mM $Fe(CN)_6^{-4/-3}$ solutions of pH 3 and 9 while keeping the total ionic concentration constant.

Electrode Treatment and SAM Preparation. Ag ring electrodes employed for SER measurements were treated by repetitive electrochemical oxidation/reduction cycles in 0.1 M KCl to create a SER-active nanostructured surface.

Au electrodes used for CV and EIS were first oxidized in 10% $HClO_4$ by applying a potential of 2.5 V for 2 min, then sonicated in HCl 10% for 15 min and rinsed with water. Subsequently, the electrodes were treated with 3:1 v/v H_2O_2:H_2SO_4 mixture at 120 °C, followed by potential cycling between −0.2 and +1.6 V in 10% $HClO_4$ and, finally, thorough washing with water and ethanol.

Electrode surface areas were determined by integration of the gold oxide reduction peak in voltammograms recorded at 0.1 V s^{-1} between −0.25 and 1.6 V in 0.5 M H_2SO_4, considering a conversion factor of 0.44 mC cm^{-2} for a gold oxide monolayer. The average surface area of the Au electrodes used in this work was calculated to be 0.18 ± 0.08 cm^2, with a roughness factor of 3.4 ± 1.1.

For coating with NH_2-terminated SAMs, the electrodes were soaked in 2 mM solutions of the corresponding thiols in acid medium (4:1 v/v C_2H_5OH-$HClO_4$ 10^{-4} M pH 4) to prevent binding through the NH_2 groups. For OH-SAMs, 2 mM solutions of the respective OH-terminated mercaptoalkanes in ethanol were employed. Mixed NH_2/OH-SAMs were prepared by mixing equal volumes of 2 mM solutions of NH_2 and OH-terminated mercaptoalkanes. Incubations were carried out at 4 °C for variable periods of time, ranging from 12 to 72 h for C2 and C16 SAMs, respectively. The studies reported in the present work do not allow discriminating phase mixing from phase separation in these SAMs. Previous work on similar systems, however, demonstrated molecular scale mixing of the two components of the SAM.[16,24] SAM-modified electrodes were kept in the darkness to prevent photochemical damage. Prior to measurements, modified electrodes were rinsed thoroughly with ethanol and water and subjected to CV in Pi buffer or KCl solution as conditioning treatment.[25]

RESULTS AND DISCUSSION

Chemical Characterization of the SAMs. The chemical composition of NH_2-C6 and NH_2-C11 SAMs on Au was analyzed by recording high-resolution XPS spectra. Figure 1 shows (a) N 1s, (b) C 1s, and (c) S 2p XP spectra corresponding to the bare gold substrate and NH_2-C6 and NH_2-C11 self-assembled monolayers from bottom to top. The bare Au substrate shows no N 1s, C 1s, and S 2p XP signals,

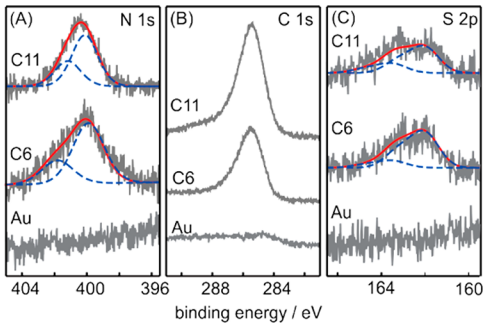

Figure 1. XPS spectra of bare and NH_2-SAMs modified gold electrodes. (A) N 1s, (B) C 1s, and (C) S 2p.

dx.doi.org/10.1021/la304730q | Langmuir 2013, 29, 5351−5359

corroborating that the initial state of the crystal prior monolayer formation corresponds to a clean Au surface. For both SAMs, S 2p spectra exhibit a spin doublet at binding energies (BE) of 162.0 and 163.2 eV as main component, which have been assigned to S 2p3/2 and S 2p1/2, respectively, for metal-bound thiol species.[26] The fitting procedures reveal minor fractions of unbound thiols (S 2p BE of 163.5 eV) that account for less than 20% of the total S 2p signals, whereas signals corresponding to oxidized sulfur species (S 2p BE >166 eV) were not detected, thereby indicating that our preparations are largely free of N-bound and sulfonic species previously reported for comparable SAMs.[15,16] XPS C 1s spectra, which show no indication of C═O species, present asymmetric signals that can be fitted with an intense band at 285 eV and a smaller one at 286.6 eV, and are consistent with CH_2 and C−N species, respectively.[17] Finally, the asymmetric N 1s spectra can be quantitatively fitted with two bands at 399.5 and 401.4 eV, which are assigned to N−C species of neutral and protonated amine tail groups, respectively.[17,27]

Thus, qualitatively, XPS results are consistent with relatively well ordered SAMs of thiols attached to the surface through the S atom and that do not present significant oxidation of the head and tail groups. The experimentally determined C/S and N/S ratios, however, are higher than predicted by stoichiometry. This overestimation is ascribed to attenuation of the surface-bound sulfur signal due to inelastic scattering produced by the long hydrocarbon overlayer.[17]

Finally, XPS measurements indicate the presence of oxygen in the monolayer that can be ascribed to water molecules tightly bound to the amine functional group as previously reported.[17]

Table 1. XPS Determined Atomic Ratio and Degree of Protonation[a]

SAM	C/S	N/S	O/N	$NH_3^+/(NH_2 + NH_3^+)$
NH_2-C6	17 (6)	2.3 (1)	1.4 (0)	0.28
NH_2-C11	24 (11)	2.4 (1)	1.5 (0)	0.33

[a]Values in parentheses are the expected ones from the thiol stoichiometry.

Reductive Desorption. Linear sweep voltammetry (LSV) was employed for analyzing the reductive desorption of SAMs of NH_2-C*n* thiols with n = 2, 6, and 8 in alkaline medium. As shown in Figure 2 and Table 2, the potential of the reductive peak downshifts upon increasing the chain length of the alkanethiols, thereby indicating higher stability of the thicker films due to enhanced van der Waals lateral interactions. The integrated charges of the reductive waves are close to the maxima values previously reported for Au(111) electrodes coated with high coverage SAMs of different alkanethiols (75−80 μC cm^{-2}).[28] Therefore, the LSV experiments suggest relatively well packed SAMs. One should be aware, however, that several factors, such as phase transitions or changes in the capacitive currents during desorption, may contribute to overestimating surface coverage, particularly for very short chain lengths.[29] For NH_2-C*n* with n > 8, on the other hand, no reductive peak could be detected before hydrogen evolution in this medium, thus suggesting highly ordered SAMs.

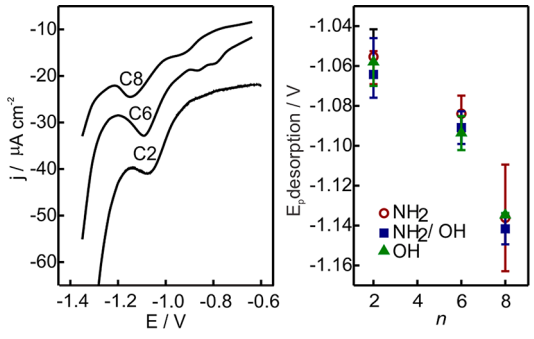

Figure 2. Reductive desorption scan at 0.02 V s^{-1} for NH_2−SAMs modified gold electrodes in 0.5 M KOH (left). Reductive desorption peak potential for SAMs of different composition as a function of the chain length (right). The bars represent standard deviations.

Reductive desorption was also investigated for single component SAMs of OH-Cn and mixed SAMs assembled from 1:1 solutions of OH-C*n* and NH_2-C*n*. The results indicate that, within experimental error, both the potentials of reductive desorption and the integrated charges are nearly independent of the nature of the substituent tail group (Figure 2 and Table 2) and only show a clear correlation with the chain lengths, thus indicating similar degrees of order for the different chemical compositions.

Capacitive Response. Single-component and 1:1 mixed SAMs of NH_2-C*n* and OH-C*n* alkanethiols (n = 2, 6, 8, 11, and 16) on Au were characterized by CV and EIS. As shown in Figure 3A for some representative examples, all these systems exhibit capacitive voltammetric responses in a relatively wide potential range around 0 V. Differential capacitances (C_d) were determined from the linear variation of the CV capacitive currents ($j_{cap} = (j_a - j_c)/2$) as a function of the potential scan rates, v (Figure 3B). In good agreement with the results obtained from reductive desorption experiments, C_d values show a clear correlation with the chain length of the SAMs but are largely independent of the chemical nature of the tail groups (Figure 3C and Table SI1).

EIS spectra taken at 0 V could be satisfactorily fitted to a Randles circuit with a constant phase element (CPE) connected in parallel to a resistance, R; all in series with the solution uncompensated resistance, R_u (Figure 4A). The contribution of a CPE to the impedance can be written as

$$Z_{CPE} = Y_0^{-1}(\omega i)^{-\alpha} \quad (1)$$

where Y_0 is a parameter related with the capacitance, ω is the angular frequency, i is the imaginary unit, and α is a fractional exponent whose value is influenced by a variety of phenomena such as roughness or inhomogeneities of the electrode surface or distributions of capacitances and relaxation times.[30] Therefore, CPEs are not necessarily associated to a unique value of capacitance but, instead, to a representative value C_0 (often called true capacitance) that can be calculated as[31]

$$C_0 = (RY_0)^{1/\alpha}/R \quad (2)$$

As shown in Table SI1, the values of α obtained for the different SAMs are close to one, which implies a behavior similar to an ideal capacitor. Moreover, the values of the impedimetric and voltammetric capacitances (C_0 and C_d, respectively) are very close and exhibit comparable dependencies with the chain lengths of the alkanethiols.

The capacitance of the SAM-coated electrodes can be regarded as a series combination of the dielectric capacitance of the film, C_{film}, and the capacitance due to the electrolyte

dx.doi.org/10.1021/la304730q | Langmuir 2013, 29, 5351−5359

Table 2. Reductive Desorption Parameters for Different SAM-Coated Au Electrodes Determined at 0.02 V s^{-1} Scan Rate in 0.5 M KOH[a]

	$Q_{des}/\mu C\ cm^{-2}$			Ep/V			fwhm/mV		
n	NH_2	NH_2/OH	OH	NH_2	NH_2/OH	OH	NH_2	NH_2/OH	OH
2	87 ± 12	121 ± 4	120 ± 5	1.06 ± 0.01	1.06 ± 0.01	1.06 ± 0.01	130 ± 10	150 ± 20	160 ± 10
6	64 ± 11	85 ± 35	79 ± 20	1.08 ± 0.01	1.09 ± 0.01	1.09 ± 0.01	120 ± 10	130 ± 20	120 ± 10
8	60 ± 26	68 ± 26	68 ± 20	1.14 ± 0.03	1.14 ± 0.01	1.13 ± 0.01	150 ± 40	160 ± 40	150 ± 40

[a]For each parameter the standard deviation from at least three different electrodes is indicated.

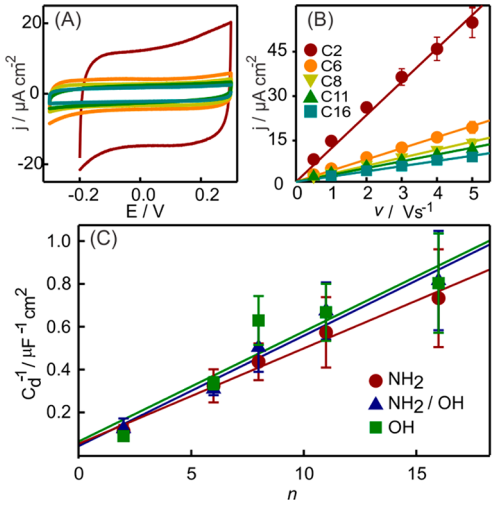

Figure 3. (A) Voltammetric response at 1 V s^{-1} in 0.01 M Pi pH 7 for NH_2-SAMs modified gold electrodes. (B) Capacitive current as a function of the sweep potential rate for NH_2-SAMs modified gold electrodes. (C) Reciprocal of the voltammetric capacitances as a function of the number of carbon atoms, *n*. Each point corresponds to the average of three different electrodes and bars to the standard deviation. Symbol code in the graphic.

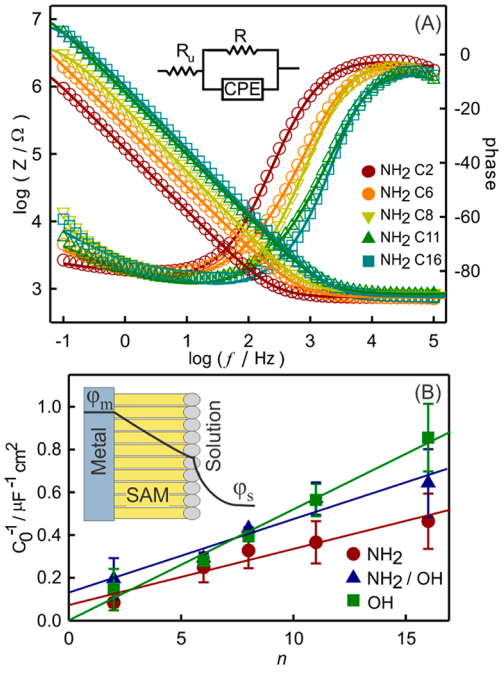

Figure 4. (A) Bode representation of EIS spectra at 0 V for NH_2SAMs of different chain length in 0.01 M Pi pH 7 (B) Reciprocal of the impedimetric capacitances as a function of the number of carbon atoms, *n*. Each point corresponds to the average of three different electrodes and bars to the standard deviation. Schematic representation of the SAM-modified electrode/solution interface inside the graphic.

solution, that within the Gouy–Chapman–Stern model is attributed to the diffuse layer (Figure 4)[32]

$$C^{-1} = C_{dif}^{-1} + C_{film}^{-1} \quad (3)$$

$$C_{dif} = \varepsilon_0 \varepsilon_r \kappa \cosh(ze\Delta\phi/2k_BT) \quad (4)$$

$$C_{film}^{-1} = d/\varepsilon_0\varepsilon_{film} \quad (5)$$

where $\Delta\phi$ is the potential difference between the outer Helmholtźs plane and the bulk solution, z is the charge of the electrolyte, e is the charge of the electron, k_B is Boltzmann's constant, T is the temperature, d is the thickness of the film, κ is the inverse of Debye's length, ε_0 is the vacuum permittivity, and ε_r and ε_{film} are the solution and film relative dielectric constants. Within this approximation, ε_{film} can be determined from the linear plots in Figures 3C and 4B as indicated in eq 6 and using $\partial d/\partial n$ = 1.28 Å/methylene:[12,33]

$$\varepsilon_{film} = \frac{(\partial d/\partial n)}{\varepsilon_0(\partial C_{film}^{-1}/\partial n)} \quad (6)$$

The values of ε_{film} obtained in these way for single-component and mixed SAMs (Table 3) are very close to those reported previously for SAMs of CH_3-terminated (1.8–2.6)[34,35] and OH-terminated (3.0–3.3)[34,36] *n*-alkylthiols, thus indicating that the monolayers are not significantly interpenetrated by the solvent. These results contrast with a recent study of NH_2-terminated SAMs that yielded a significantly larger value under similar conditions, ε_{film} = 11, which was attributed to highly wet monolayers.[12]

Table 3. Relative Dielectric Constant of the Film, ε_{film}, (Calculated by eq 6) for Different SAMs on Gold[a]

capacitance	NH_2-C*n*	NH_2/OH-C*n*	OH-C*n*
voltammetric (C_d)	3.3 (±0.5)	2.8 (±0.4)	2.8 (±0.5)
impedimetric (C_0)	5.5 (±1.0)	4.2 (±0.7)	2.5 (±0.1)

[a]Standard deviations are indicated in parentheses.

Chain Conformation. The C–S vibrational stretching mode (ν_{C-S}) of alkanethiols has been shown to constitute a sensitive reporter of the conformation of the S–C–C chain and, thus, of the order of their SAMs on coinage metals. Specifically, for the gauche conformation this band appears typically within the range 620–660 cm^{-1}, and up-shifts to ca. 690–740 cm^{-1} for the trans conformer.[37,38] Therefore, we have complemented the characterization of the different SAMs studied here with surface-enhanced Raman (SER) measurements under 514 nm excitation. For these particular experiments the thiols were assembled on Ag substrates, as Au surfaces do not provide sufficient enhancement for the Raman

dx.doi.org/10.1021/la304730q | Langmuir 2013, 29, 5351–5359

signals to be detected. Structural differences of SAMs on Ag and Au, such as tilt angles of the thiols, are well documented and, therefore, SER and electrochemical experiments cannot be compared quantitatively. However, as shown in previous studies of SAMs on Ag, Au and Cu, tendencies regarding gauche/trans content as a function of chain length are expected to be qualitatively similar,[39] thus providing valuable information in this respect.

Representative SER spectra of single component and mixed SAMs of NH_2-C*n* and OH-C*n* are shown in Figures 5, SI1, and

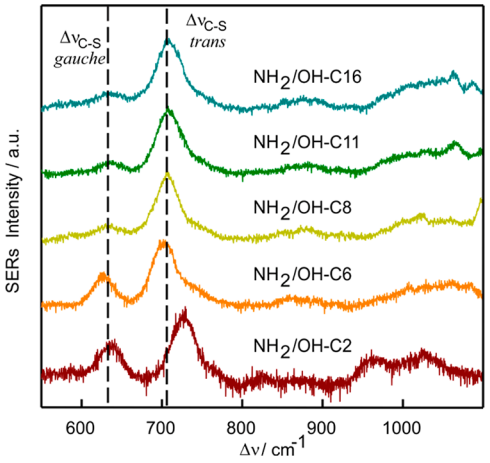

Figure 5. SER spectra of NH_2/OH-terminated SAMs of different chain length. Spectra were scaled to the same intensity of trans band.

SI2. The region between 950 and 1100 cm^{-1} presents multiple bands that correspond to C−C modes that do not provide straightforward structural information. The lower frequency region, instead, is characterized by two bands at ca. 630 and 700 cm^{-1}, which are assigned to the ν_{C-S} bands of the gauche and trans conformations, respectively.[37,38] Note that the overall spectral appearance, particularly in the ν_{C-S} region, is largely insensitive to the nature of the tail groups and, instead, the normalized gauche intensity $I_G/(I_G + I_T)$ decreases with the chain lengths of the thiols (Figure 6), thus indicating better ordered structures for the thicker films. In agreement with previous studies,[37,39,40] the positions of the ν_{C-S} bands show only marginal variations with the chain lengths, except for NH_2-C2 and OH-C2 SAMs that present a ca. 20 cm^{-1} upshift of the trans conformer (Figure SI 3). Moreover, in all cases SER

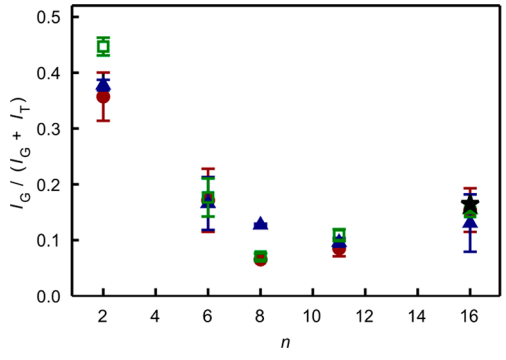

Figure 6. Normalized gauche intensity for different chain length. NH_2-SAMs (circles), NH_2/OH-SAMs (triangles), and OH-SAMs (squares). Value obtained for a 1-hexadecanethiol SAM was added for comparison (black star).

spectra show no indication of unbound or oxidized sulfur species[37,41]

Thus vibrational spectroscopic data on Ag show excellent agreement with the results obtained by XPS, LSV, CV, and EIS for equivalent SAMs on Au.

Potential cycling of the coated electrodes results in decreased $I_G/(I_G + I_T)$ (Figure SI 4), thus indicating that this method improves the order of the SAMs as previously proposed for other thiols.[25] The effect is very pronounced for the thinner films (C2-SAMs) and almost imperceptible for the thicker ones (C16-SAMs).

Surface pK_a. The acid−base properties of NH_2-C*n* SAMs on Au were characterized by CV and EIS titrations employing the couple $Fe(CN)_6^{-3/-4}$ as molecular probe, which was chosen because its formal reduction potential is nearly pH-independent within the range of interest (Figure 7A).

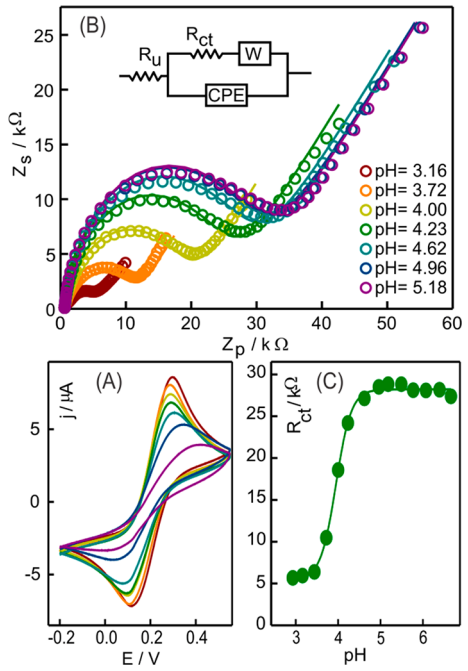

Figure 7. (A) CV at 0.05 V s^{-1} and (B) Nyquist's plots of a NH_2-C16 electrode in the presence of 1 mM $Fe(CN)_6^{-3/-4}$ in 0.01 M phosphate of different pH at 0.2 V. Solid lines correspond to fits to the equivalent circuit depicted in this Figure. (C) Charge transfer resistance values as a function of the solution pH. Line corresponds to the sigmoidal fit.

The heterogeneous redox reaction of the soluble probe may occur either by direct electron tunneling through the alkyl chains or by diffusion through pinholes and defects present in the SAMs.[42] Long chain aliphatic thiols form highly packed monolayers on Au, which are essentially free of measurable defects, thereby acting as a barrier to ion penetration. Moreover, given that the electron tunneling probability scales with the square of the electronic matrix element that, in turn, decays exponentially with the SAM thickness, direct ET of soluble species is essentially blocked for such systems.[43−45] As shown in Figure 7A, NH_2-C16 SAMs do not block the ET reaction completely at the higher pH values explored, although the voltammograms are characterized by relatively small peak currents and large peak separations that are indicative of a slow process. Hence, these results suggest a convolution of through-SAM superexchange and partial penetration of the probe through gaps present in the monolayers. As the solution pH is

dx.doi.org/10.1021/la304730q | Langmuir 2013, 29, 5351−5359

lowered, peak separations decrease concomitantly with a significant increase of the peak currents. Most likely this effect arises from the protonation of the amine tail groups, which results in (i) the monolayers becoming less compact due to electrostatic repulsion of the functional groups and (ii) higher surface concentrations of the negatively charged redox probe.

Typical Nyquist plots obtained for NH_2-C16 SAMs within the frequency range 10^5−10^{-1} Hz as a function of pH are shown in Figure 7B. In these representations the radii of the semicircles are direct measures of the charge-transfer resistance, R_{ct}, as a function of the pH of the bulk solution. The underlying changes in the electrochemical reaction kinetics can be primary ascribed to modulation of the potential at the outer Helmholtz plane and, therefore, of the electrostatic interactions between the surface and the molecular probe, due to pH-dependent variation of the charge density at the inner Helmholtz plane, i.e., of the protonation degree of the NH_2 groups.[50] All EIS data could be satisfactorily fitted to a Randles equivalent circuit using a constant phase element to model the double layer capacitance and a Warburg element (W) to account for the diffusion of the electroactive probe.[40] The R_{ct} values extracted from this analysis exhibit sigmoidal dependencies with the solution pH (Figure 7C), which allow for the determination of apparent pK_a values by fitting the data to eq 7:

$$R_{ct} = R_{ct,0} + \Delta R/(1 + 10^{-pH=pK_{a,app}/n_{app}}) \quad (7)$$

As summarized in Figure 8 and Table SI2, the obtained pK_a's show an inverse correlation with the chain length of the NH_2-C*n* SAMs that can be described in terms of a sigmoidal function that approaches the pK_a value of primary alkylamines in solution as *n* tends to zero. The decrease of the apparent pK_a's of the amines in the assemblies has a complex multicausal origin, but can be rationalized in terms of the interplay of electrostatic and hydrophobic interactions as main contributions. Within this rationale, lateral attractive van der Waals forces are expected to become stronger as *n* increases, thus rendering more compact SAMs and, thereby, reinforced electrostatic repulsions between protonated groups that result in lower pK_a values. In good agreement with this interpretation, apparent pK_a's increase with parameters of disorder such as the fraction of S−C−C chains in the gauche conformation.

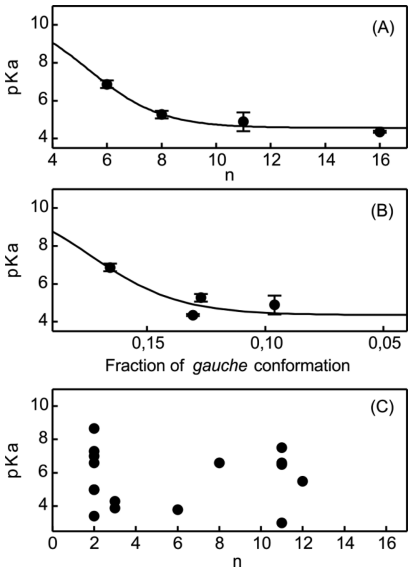

Figure 8. Apparent pK_a values of NH_2-SAMs as a function of the chain length (A) and as a function of the normalized gauche intensity (B) obtained in the present work. Panel C shows apparent pK_a values reported NH_2-SAMs reported in the literature.[33,46−56] See Table SI3 for further details.

Mixed SAMs obtained from 1:1 solutions of OH-C*n* and NH_2-C*n* exhibit only a small increase of the apparent pK_a (ca. 0.5 pH units) with respect to the corresponding single component NH_2-C*n* SAMs (Table SI2). On the other hand, the results obtained using phosphate and perchlorate electrolyte solutions are similar within experimental error (Figure SI5).

Note that, in sharp contrast with the clear correlations found here, pK_a values of NH_2-C*n* SAMs reported previously exhibit large dispersions that, when taken together, span over 6 pH units for single chain lengths and show no evident dependence with the number of methylene groups (Figure 8C).

Specific Adsorption of Inorganic and Organic Phosphate. In previous work we have reported that inorganic phosphate (Pi: phosphate buffer, pH 7) and ATP anions are able to mediate high affinity binding of the basic protein Cyt on electrodes coated with NH_2-terminated SAMs. Moreover, the results showed that the bound protein preserves the native folding and presents an average orientation that allows for efficient direct electrochemistry.[22] While the specificity of the phosphate species was unambiguously demonstrated, it was not clear though whether the effect arises exclusively from binding of Pi and ATP to specific sites on the protein surface followed by unspecific electrostatic adsorption of the complexes to the positively charged SAMs, or possible specific adsorption of the phosphate species to the SAMs also plays a role. Therefore, we have employed EIS to investigate the interactions of Pi and ATP with single component NH_2-C*n* SAMs and with 1:1 mixtures of OH-Cn and NH_2-C*n* on Au (*n* = 6 and 11). The determinations were performed employing $Fe(CN)_6^{-3/-4}$ as redox probe in buffer HEPES (pH 7) containing 0.5 M KCl to maintain the ionic strength approximately constant. The addition of increasing amounts of Pi and ATP has no effect on the formal reduction potential of the $Fe(CN)_6^{-3/-4}$ couple, but it results in a significant increase of the charge transfer resistance (R_{ct}) as verified by the larger separations of the anodic and cathodic voltammetric peaks and by the increased radii of the semicircles in the Nyquisťs plots (Figure 9). Representative examples of R_{ct} values obtained by nonlinear fitting of the Nyquist's plots to a Randles equivalent circuit are plotted in Figures 10 and SI6−8 as a function of the concentrations of the phosphate species. The results are consistent with the specific adsorption of Pi and ATP to the SAMs, thereby overcompensating the positive charges of the amino tail groups and, thus, hindering the approximation of the negatively charged redox probe to the surface. In agreement with this interpretation, R_{ct} values determined for the positively charged redox couple $Ru(NH_3)_6^{3+/2+}$ present the opposite tendency (Figure 10), actually facilitating the interfacial ET reaction with increasing concentrations of Pi in the bulk solution. In all cases, the experimentally determined data can be reasonably fitted with eq 8 (Figures 10 and SI6−8), where $1/K_{Pi}$ is the mean equilibrium binding constant of the different phosphate species to the SAM-coated electrodes in terms of a simple Langmuir isotherm:

$$R_{ct} = R_{ct,0} + \Delta R\frac{[Pi]}{K_{Pi} + [Pi]} \quad (8)$$

dx.doi.org/10.1021/la304730q | *Langmuir* 2013, 29, 5351−5359

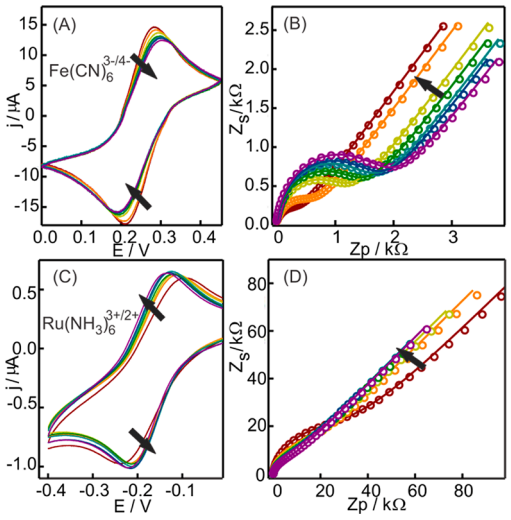

Figure 9. Electrochemistry of a NH_2C11 SAM-modified gold electrode in 1 mM $Fe(CN)_6^{-3/-4}$ (top) and 0.1 mM $Ru(NH_3)_6^{3+/2+}$(bottom) in 0.5 M KCl HEPES 1 mM pH 7 with different concentrations of Pi. Arrows indicate increasing Pi concentration from 0 to 60 mM. CV at 0.05 V s^{-1} (A, C) and EIS spectra between 10^4 and 0.15 Hz at 0.25 V (B) and −0.2 V (D). Solid lines correspond to the fit to circuit in panel A.

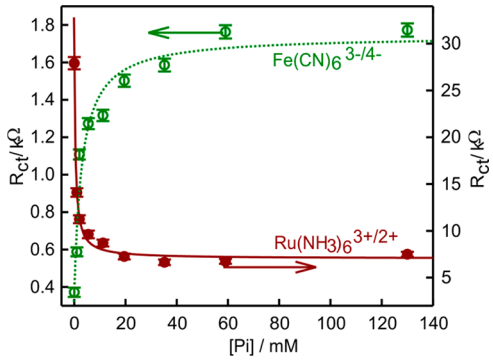

Figure 10. Charge transfer resistance in the presence of two redox probes as a function of the Pi bulk concentration. Solid lines correspond to fittings to eq 8.

As summarized in Table 4, the affinity of Pi for single component NH_2-C*n* SAMs is close to 1 mM, independently of the chain length of the thiol, but it drops by a factor of ca. 30 for 1:1 mixed SAMs of OH-C*n*/NH_2-C*n*. Thus, given that the pK_a values determined for single component and mixed SAMs of equal length are nearly identical and that the EIS binding experiments were performed at high ionic strength, it can be concluded that Pi ions adsorb specifically to the NH_2-containing SAMs. Qualitatively similar conclusions are obtained for ATP, although in these case affinities are even higher (Table 4 and Figure SI8).

Table 4. Phosphate Species Affinity Constants for Amino-Terminated SAMs

	K_{Pi}/mM		K_{ATP}/mM	
N	NH_2	NH_2/OH	NH_2	NH_2/OH
C6	1.2 (±0.3)	44 (±16)	0.1 (±0.09)	11 (±3)
C11	1.6 (±0.4)/ 0.6 (±0.1)[a]	37 (±6)/ 5 (±2)[a]	1.1 (±0.3)	2.7 (±0.7)

[a]Values determined with $Ru(NH_3)_6^{3+/2+}$ as redox probe, the other values were measured with $Fe(CN)_6^{3-/4-}$. Standard errors of the fit are presented in brackets. Data of two electrodes were averaged before fitting.

In excellent agreement with these results, SERR titration experiments showed half maxima of Cyt adsorption to NH_2-C6 SAMs at Pi and ATP concentrations of approximately 3 and 0.5 mM, respectively. On the other hand, the affinity of Cyt for NH_2-C6 SAMs in the presence of 10 mM Pi, has been found to be in the submicromolar range.[22] Therefore it can be concluded that phosphate mediated binding of Cyt to NH_2-terminated SAMs relies upon specific interactions of Pi and ATP with the surfaces of both the protein and the SAM-coated electrodes.

The apparent rate constant of Pi-mediated heterogeneous ET of Cyt on NH_2-terminated SAMs exhibits the characteristic exponential dependence with the chain length of the SAMs for $n > 10$, but it levels off for thinner films. In analogy with conclusions obtained from detailed theoretical and experimental studies of Cyt on COOH-terminated SAMs, these findings were interpreted in terms of an interplay between protein and interfacial water dynamics with tunneling probabilities.[22] At long distances electron tunneling is considered the rate-limiting event. Upon shortening the chain length of the thiols high and low amplitude motion of the adsorbed protein and of interfacial water molecules in search for efficient electron pathways become determinant. The present results strongly support this hypothesis. In the plateau region ($n < 10$) the apparent ET rate constant of Cyt on single component NH_2-C*n* SAMs is 1 order of magnitude lower than on 1:1 OH-C*n*/NH_2-C*n* mixtures (Figure SI9). This is consistent with the fact that NH_2−Cn SAMs show significantly larger affinity for Pi (Table 4) and, therefore, a higher charge density at the interface that impairs protein and solvent dynamics. Within this interpretation, as the Pi affinity for NH_2-terminated SAMs is independent of the chain length (Table 4), the apparent rate constant of the redox reaction is expected to be reasonably well described as $k_{app}^{-1} = k_{ET}^{-1} + k_r^{-1}$, where $k_{ET} = k_0 \exp(-\beta n)$ is the distance-dependent rate constant for nonadiabatic ET, $\beta \approx 1.1/CH_2$ is the tunneling decay parameter and k_r is the distance-independent rate constant of rearrangement of protein and interfacial water molecules. As an indication of consistency, the experimentally k_{app} vs *n* plots can be fitted reasonably well with this sequential kinetic model (Figure SI9).

CONCLUSIONS

We have shown that chemisorption from solutions of NH_2-terminated alkanethiols on Au leads to relatively well ordered SAMs that are essentially free of oxidized head and tail functional groups. Reductive desorption, EIS and SER experiments showed that the degree of order increases with the chain length of the alkanethiols, but it is largely insensitive to dilution with OH-terminated thiols. Average dielectric constants of the films exhibited small values consistent with low penetration of water molecules. Impedimetric titrations revealed clear correlations of the apparent surface pK_a values with the chain lengths and conformations of the alkanethiols in the assemblies, thus indicating that electrostatic repulsions between protonated groups, which are reinforced in the better ordered thick films, result in lower pK_a values as *n* increases.

Binding EIS studies demonstrated specific adsorption of inorganic phosphate and ATP species that lead to over-compensation of the surface charges thereby mediating adsorption of positively charged macromolecules. Moreover,

dx.doi.org/10.1021/la304730q | *Langmuir* 2013, 29, 5351−5359

the results showed that immobilization and ET dynamics of the basic protein cytochrome *c* on electrodes coated with NH_2-terminated alkanethiols can be modulated through the surface concentration of specifically adsorbed phosphate species.

■ ASSOCIATED CONTENT

Supporting Information

Capacitive parameters of the SAMs together with the determined and bibliographic pK_a values are listed in Tables SI1−SI3. Additional data of SERs, proton and phosphate binding, and Cyt ET kinetics on these SAMs are presented and analyzed in Figures SI1−SI9. This material is available free of charge via the Internet at http://pubs.acs.org.

■ AUTHOR INFORMATION

Corresponding Author

*Fax: +54 (11) 4576-3341. E-mail dhmurgida@qi.fcen.uba.ar.

Notes

The authors declare no competing financial interest.

■ ACKNOWLEDGMENTS

W.A.M. and D.A.C. are thankful for a fellowship of CONICET. Financial support by ANPCyT (PICT 2010-070 and PICT 2011-1249) and UBA (UBACYT 20020090100094) is gratefully acknowledged. F.J.W. and D.H.M. are members of CONICET.

■ REFERENCES

(1) Love, J. C.; Estroff, L. A.; Kriebel, J. K.; Nuzzo, R. G.; Whitesides, G. M. Self-assembled monolayers of thiolates on metals as a form of nanotechnology. *Chem. Rev.* **2005**, *105*, 1103−69.

(2) Gooding, J. J.; Ciampi, S. The molecular level modification of surfaces: from self-assembled monolayers to complex molecular assemblies. *Chem. Soc. Rev.* **2011**, *40*, 2704−18.

(3) Zhang, J.; Chi, Q.; Hansen, A. G.; Jensen, P. S.; Salvatore, P.; Ulstrup, J. Interfacial electrochemical electron transfer in biology - towards the level of the single molecule. *FEBS Lett.* **2012**, *586*, 526−35.

(4) Koepsel, J. T.; Murphy, W. L. Patterned self-assembled monolayers: efficient, chemically defined tools for cell biology. *ChemBioChem* **2012**, *13*, 1717−24.

(5) Murgida, D. H.; Hildebrandt, P. Disentangling interfacial redox processes of proteins by serr spectroscopy. *Chem. Soc. Rev.* **2008**, *37*, 937−945.

(6) Ulman, A. Formation and structure of self-assembled monolayers. *Chem. Rev.* **1996**, *96*, 1533−1554.

(7) Pensa, E.; Cortés, E.; Corthey, G.; Carro, P.; Vericat, C.; Fonticelli, M. H.; Benítez, G.; Rubert, A. a; Salvarezza, R. C.; Corte, E. The chemistry of the sulfur-gold interface: in search of a unified model. *Acc. Chem. Res.* **2012**, *45*, 1183−92.

(8) Shyue, J.-J.; De Guire, M. R. Single-step preparation of mesoporous, anatase-based titanium-vanadium oxide and its application. *J. Am. Chem. Soc.* **2005**, *127*, 12736−42.

(9) Shyue, J.; Guire, M. R. De Deposition of vanadium (v) oxide thin films on nitrogen-containing self-assembled monolayers. *Chem. Mater.* **2005**, *17*, 787−794.

(10) Kuo, C.-W.; Lai, J.-J.; Wei, K. H.; Chen, P. Surface modified gold nanowires for mammalian cell transfection. *Nanotechnology* **2008**, *19*, 025103.

(11) Oh, S. J.; Cho, S. J.; Kim, C. O.; Park, J. W. Characteristics of dna microarrays fabricated on various aminosilane layers. *Langmuir* **2002**, *18*, 7223−7228.

(12) Chou, A.; Eggers, P. K.; Paddon-Row, M. N.; Gooding, J. J. Self-assembled carbon nanotube electrode arrays: effect of length of the linker between nanotubes and electrode. *J. Phys. Chem. C* **2009**, *113*, 3203−3211.

(13) Shein, J. B.; Lai, L. M. H.; Eggers, P. K.; Paddon-Row, M. N.; Gooding, J. J. Formation of efficient electron transfer pathways by adsorbing gold nanoparticles to self-assembled monolayer modified electrodes. *Langmuir* **2009**, *25*, 11121−8.

(14) Jensen, P. S.; Chi, Q.; Grumsen, F. B.; Abad, J. M.; Horsewell, A.; Schiffrin, D. J.; Ulstrup, J. Gold nanoparticle assisted assembly of a heme protein for enhancement of long-range interfacial electron transfer. *J. Phys. Chem. C* **2007**, *111*, 6124−6132.

(15) Wang, H.; Chen, S.; Li, L.; Jiang, S. Improved method for the preparation of carboxylic acid and amine terminated self-assembled monolayers of alkanethiolates. *Langmuir* **2005**, *21*, 2633−6.

(16) Li, L.; Chen, S.; Jiang, S. Molecular-scale mixed alkanethiol monolayers of different terminal groups on au(111) by low-current scanning tunneling microscopy. *Langmuir* **2003**, *19*, 3266−3271.

(17) Baio, J. E.; Weidner, T.; Brison, J.; Graham, D. J.; Gamble, L. J.; Castner, D. G. Amine terminated sams: investigating why oxygen is present in these films. *J. Electron Spectrosc. Relat. Phenom.* **2009**, *172*, 2−8.

(18) Campiña, J. M.; Martins, A.; Silva, F. Probing the organization of charged self-assembled monolayers by using the effects of ph, time, electrolyte anion, and temperature, on the charge transfer of electroactive probes. *J. Phys. Chem. C* **2009**, *113*, 2405−2416.

(19) Campiña, J. M.; Martins, A.; Silva, F. Selective permeation of a liquidlike self-assembled monolayer of 11-amino-1-undecanethiol on polycrystalline gold by highly charged electroactive probes. *J. Phys. Chem. C* **2007**, *111*, 5351−5362.

(20) Yu, Q.; Golden, G. Probing the protein orientation on charged self-assembled monolayers on gold nanohole arrays by sers. *Langmuir* **2007**, *23*, 8659−8662.

(21) Chen, X.; Ferrigno, R.; Yang, J.; Whitesides, G. M. Redox properties of cytochrome c adsorbed on self-assembled monolayers: a probe for protein conformation and orientation. *Langmuir* **2002**, *18*, 7009−7015.

(22) Capdevila, D. A.; Marmisollé, W. A.; Williams, F. J.; Murgida, D. H.; Marmisolle, W. A. Phosphate mediated adsorption and electron transfer of cytochrome c a time-resolved serr spectroelectrochemical study. *Phys. Chem. Chem. Phys.* **2013**, 1−9.

(23) Murgida, D. H.; Hildebrandt, P. Heterogeneous electron transfer of cytochrome c on coated silver electrodes electric field effects on structure and redox potential. *J. Phys. Chem. B* **2001**, *105*, 1578−1586.

(24) Lin, W.-C.; Lee, S.-H.; Karakachian, M.; Yu, B.-Y.; Chen, Y.-Y.; Lin, Y.-C.; Kuo, C.-H.; Shyue, J.-J. Tuning the surface potential of gold substrates arbitrarily with self-assembled monolayers with mixed functional groups. *Phys. Chem. Chem. Phys.* **2009**, *11*, 6199−6204.

(25) Tanimura, R.; Hill, M. G.; Margoliash, E.; Niki, K.; Ohno, H.; Gray, H. B. Active carboxylic acid-terminated alkanethiol self-assembled monolayers on gold bead electrodes for immobilization of cytochromes c. *Electrochem Solid-State Lett* **2002**, *5*, E67.

(26) Castner, D. G.; Hinds, K.; Grainger, D. W. X-ray photoelectron spectroscopy sulfur 2p study of organic thiol and disulfide binding interactions with gold surfaces. *Langmuir* **1996**, *12*, 5083−5086.

(27) Song, X.; Ma, Y.; Wang, C.; Dietrich, P. M.; Unger, W. E. S.; Luo, Y. Effects of protonation, hydrogen bonding, and photodamaging on x-ray spectroscopy of the amine terminal group in aminothiolate monolayers. *J. Phys. Chem. C* **2012**, *116*, 12649−12654.

(28) Cortés, E.; Rubert, A. A.; Benitez, G.; Carro, P.; Vela, M. E.; Salvarezza, R. C. Enhanced stability of thiolate self-assembled monolayers (sams) on nanostructured gold substrates. *Langmuir* **2009**, *25*, 5661−6.

(29) Kakiuchi, T.; Usui, H.; Hobara, D. Voltammetric properties of the reductive desorption of alkanethiol self-assembled monolayers from a metal surface. *Langmuir* **2002**, *18*, 5231−5238.

(30) Sluyters-Rehbach, M. Impedances of electrochemical systems: terminology, nomenclature and representation. *Pure Appl. Chem.* **1994**, *66*, 1831−1891.

(31) Orazem, M. E.; Shukla, P.; Membrino, M. A. Extension of the measurement model approach for deconvolution of underlying

distributions for impedance measurements. *Electrochim. Acta* **2002**, *47*, 2027−2034.
(32) Bard, A. J.; Faulkner, L. R. *Electrochemical Methods. Fundamentals and Applications*, 2nd ed.; Harris, D., Swain, E., Eds.; Wiley: New York, 2001; p 835.
(33) Fears, K. P.; Creager, S. E.; Latour, R. A. Determination of the surface pk of carboxylic- and amine-terminated alkanethiols using plasmon resonance spectroscopy. *Langmuir* **2008**, *24*, 837−843.
(34) Sondag-Huethorst, J.; Fokkink, L. Electrochemical characterization of functionalized alkanethiol monolayers on gold. *Langmuir* **1995**, 2237−2241.
(35) Porter, M.; Bright, T.; Allara, D.; Chidsey, C. E. D. Organized molecular assemblies 4 structural characterization of n-alkyl thiol monolayers on gold by optical ellipsometry, infrared spectroscopy, and electrochemistry. *J. Am. Chem. Soc.* **1987**, *109*, 3559−3568.
(36) Miller, C.; Cuendet, P.; Grätzel, M. Adsorbed w- hydroxy thiol monolayers on goid electrodes: evidence for electron tunneling to redox species in solution. *J. Phys. Chem.* **1991**, *95*, 877−886.
(37) Bryant, M. A.; Pemberton, J. E. Surface raman scattering of self-assembled monolayers formed from 1-alkanethiols at ag. *J. Am. Chem. Soc.* **1991**, *113*, 3629−3637.
(38) Bryant, M. A.; Pemberton, J. E. Surface raman scattering of self-assembled monolayers formed from 1-alkanethiols: behavior of films at au and comparison to films at ag. *J. Am. Chem. Soc.* **1991**, *113*, 8284−8293.
(39) Kudelski, A. Chemisorption of 2-mercaptoethanol on silver, copper, and gold: direct raman evidence of acid-induced changes in adsorption/desorption equilibria. *Langmuir* **2003**, *19*, 3805−3813.
(40) Michota, A.; Kudelski, A.; Bukowska, J. Chemisorption of cysteamine on silver studied by surface-enhanced raman scattering. *Langmuir* **2000**, *16*, 10236−10242.
(41) Schoenfisch, M. H.; Pemberton, J. E. Air stability of alkanethiol self-assembled monolayers on silver and gold surfaces. *J. Am. Chem. Soc.* **1998**, *120*, 4502−4513.
(42) Liu, B.; Bard, A. J.; Mirkin, M. V; Creager, S. E. Electron transfer at self-assembled monolayers measured by scanning electrochemical microscopy. *J. Am. Chem. Soc.* **2004**, *126*, 1485−1492.
(43) Becka, A. M.; Miller, C. J. Electrochemistry at omega-hydroxy thiol coated electrodes 3 voltage independence of the electron tunneling barrier and measurements of redox kinetics at large overpotentials. *J. Phys. Chem.* **1992**, *96*, 2657−2668.
(44) Xu, J.; Li, H.; Zhang, Y. Relationship between electronic tunneling coefficient and electrode potential investigated by using self-assembled alkanethiol monolayers on gold electrodes. *J. Phys. Chem.* **1993**, *97*, 11497−11500.
(45) Slowinski, K.; Chamberlain, R. V; Miller, C. J.; Majda, M. Through-bond and chain-to-chain coupling two pathways in electron tunneling through liquid alkanethiol monolayers on mercury electrodes. *J. Am. Chem. Soc.* **1997**, *119*, 11910−11919.
(46) Cao, X.-W. Study of electrode potential effect on acid−base behavior of ω-functionalized self-assembled monolayers using fourier transform surface-enhanced raman scattering spectroscopy. *J. Raman Spectrosc.* **2005**, *36*, 250−256.
(47) Nishiyama, K.; Kubo, A.; Ueda, A.; Taniguchi, I. Surface pka of amine-terminated self-assembled monolayers evaluated by direct observation of counter anion by ft-surface enhanced raman spectroscopy. *Chem. Lett.* **2002**, *31*, 80−81.
(48) Van Der Vegte, E. W.; Hadziioannou, G. Acid-base properties and the chemical imaging of surface-bound functional groups studied with scanning force microscopy. *J. Phys. Chem. B* **1997**, *101*, 9563−9569.
(49) Scavetta, E.; Solito, A. G.; Demelas, M.; Cosseddu, P.; Bonfiglio, A. Electrochemical characterization of self assembled monolayers on flexible electrodes. *Electrochim. Acta* **2012**, *65*, 159−164.
(50) Molinero, V.; Calvo, E. J. Electrostatic interactions at self assembled molecular films of charged thiols on gold. *J. Electroanal. Chem.* **1998**, *445*, 17−25.
(51) Munakata, H.; Oyamatsu, D.; Kuwabata, S. Effects of omega-functional groups on ph-dependent reductive desorption of alkanethiol self-assembled monolayers. *Langmuir* **2004**, *20*, 10123−8.
(52) Wallwork, M. L.; Smith, D. A.; Zhang, J.; Kirkham, J.; Robinson, C. Complex chemical force titration behavior of amine-terminated self-assembled monolayers. *Langmuir* **2001**, *17*, 1126−1131.
(53) Vezenov, D. V.; Noy, A.; Rozsnyai, L. F.; Lieber, C. M. Force titrations and ionization state sensitive imaging of functional groups in aqueous solutions by chemical force microscopy. *J. Am. Chem. Soc.* **1997**, *119*, 2006−2015.
(54) Degefa, T. H.; Schön, P.; Bongard, D.; Walder, L. Elucidation of the electron transfer mechanism of marker ions at sams with charged head groups. *J. Electroanal. Chem.* **2004**, *574*, 49−62.
(55) Chatelier, R. C.; Drummond, C. J.; Chan, D. Y. C.; Vasic, Z. R.; Gengenbach, T. R.; Griesser, H. J. Theory of contact angles and the free energy of formation of ionizable surfaces: application to heptylamine radio-frequency plasma-deposited films. *Langmuir* **1995**, *11*, 4122−4128.
(56) Schweiss, R.; Werner, C.; Knoll, W. Impedance spectroscopy studies of interfacial acid-base reactions of self-assembled monolayers. *J. Electroanal. Chem.* **2003**, *540*, 145−151.

Supporting Information

for

Self-Assembled Monolayers of NH_2-Terminated Thiolates: Order, pKa and Specific Adsorption

*Waldemar A. Marmisollé, Daiana A. Capdevila, Ezequiel de la Llave, Federico J. Williams and Daniel H. Murgida**

Departamento de Química Inorgánica, Analítica y Química Física and INQUIMAE. Facultad de Ciencias Exactas y Naturales, Universidad de Buenos Aires and CONICET. Ciudad Universitaria, pab. 2, piso 3, C1428EHA-Buenos Aires, Argentina.

*To whom correspondence should be adresses

Table SI1. Capacitive parameters for SAMs on gold.

n	Cd / μF cm^{-2}			C_0 / μF cm^{-2}			α		
	NH_2	NH_2/OH	OH	NH_2	NH_2/OH	OH	NH_2	NH_2/OH	OH
2	8.9 (±2.2)	8.1 (±3.1)	11.2 (±0.9)	11.9 (±3.0)	19.8 (±5.1)	19.5 (±3.1)	0.92 (±0.02)	0.94 (±0.02)	0.88 (±0.06)
6	3.1 (±0.7)	3.2 (±0.3)	3.0 (±0.3)	4.0 (±1.1)	7.1 (±0.4)	6.7 (±1.2)	0.94 (±0.01)	0.95 (±0.03)	0.95 (±0.02)
8	2.3 (±0.5)	2.0 (±0.5)	1.6 (±0.5)	3.0 (±0.8)	5.4 (±0.6)	6.3 (±1.4)	0.94 (±0.03)	0.92 (±0.06)	0.93 (±0.02)
11	1.7 (±0.5)	1.5 (±0.3)	1.5 (±0.3)	2.7 (±0.7)	3.7 (±0.9)	4.6 (±1.7)	0.89 (±0.02)	0.95 (±0.02)	0.94 (±0.03)
16	1.4 (±0.4)	1.2 (±0.3)	1.2 (±0.3)	2.2 (±0.6)	2.5 (±0.7)	3.7 (±0.8)	0.89 (±0.06)	0.93 (±0.01)	0.92 (±0.01)

Standard deviations of three electrodes are in brackets

Table SI2. Acid-Base parameters of NH_2 and NH_2/OH-termianted SAMs.

SAM	$pK_{a,app}$	
	0.01M Pi	0.01M $NaClO_4$
NH_2-C6	6.86(±0.20)	-
NH_2/OH -C6	-	7.22 (±0.01)
NH_2-C8	5.27(±0.20)	-
NH_2-C11	4.89(±0.50)	-
NH_2-C16	4.45(±0.05)*	4.31(±0.05)*
NH_2/OH-C16	4.96(±0.09)*	4.37(±0.05)*

Standard deviations of 3 electrodes are in brackets.*Standard errors of the fit are presented in brackets. Data of two electrodes were averaged before fitting.

Table SI3. Reported p*K*a values for amino-terminated SAMs in literature

NH_2- SAM	Apparent pKa	Method
NH_2-C2	3.4 to 5	FT-SERs[1]
NH_2-C2	5	FT-SERs[2]
NH_2-C2	7	Chemical force titration[3]
NH_2-C2	7.3	Faradaic Impedance titration[4]
NH_2-C2	8.7	Faradaic Impedance titration[5]
NH_2-C2,C8,C11	6.4 to 6.8	Reductive desorption[6]
NH_2-C2, C11	3	Chemical force titration[7]
NH_2-C3	3.9	Chemical force titration[8]
NH_2-C3	4.3	Contact angle[8]
NH_2-C6	3.8	FT-SERs[2]
NH_2-C7	≈6	Contact angle[9]
NH_2-C11	6.5	SPRs[10]
NH_2-C11	7.5	Faradaic voltammetry titration (DPV)[11]
NH_2-C12	5.5	Capacitive impedance titration[12]

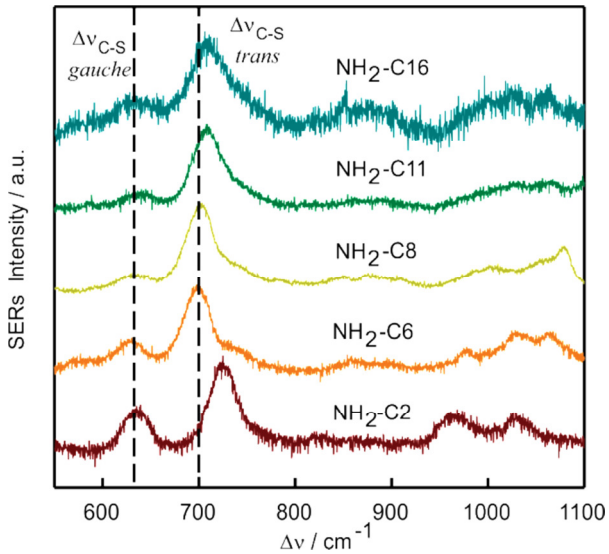

Figure SI 1. SER spectra of amino-terminated SAMs of different chain length. Spectra were scaled to the same intensity of *trans* band.

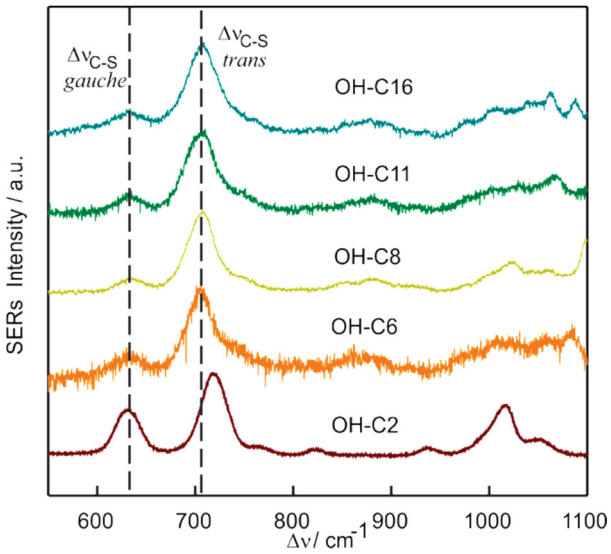

Figure SI 1. SER spectra of OH-terminated SAMs of different chain length. Spectra were scaled to the same intensity of *trans* band.

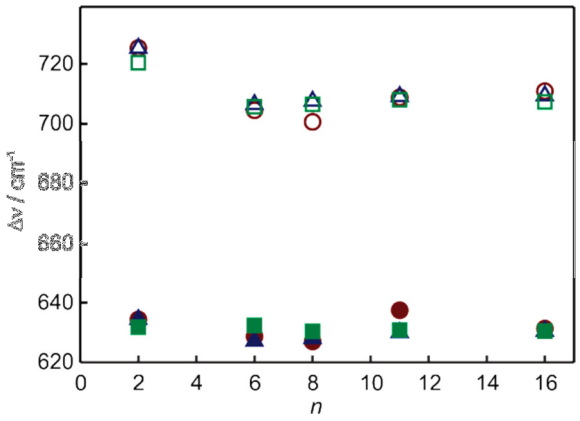

Figure SI 2. Band position of C–S stretching modes of *gauche* (full symbols) and *trans* forms (empty symbols) of SAMs of different chain length: NH_2-SAMs (circles), NH_2/OH-SAMs (triangles), OH-SAMs (squares).

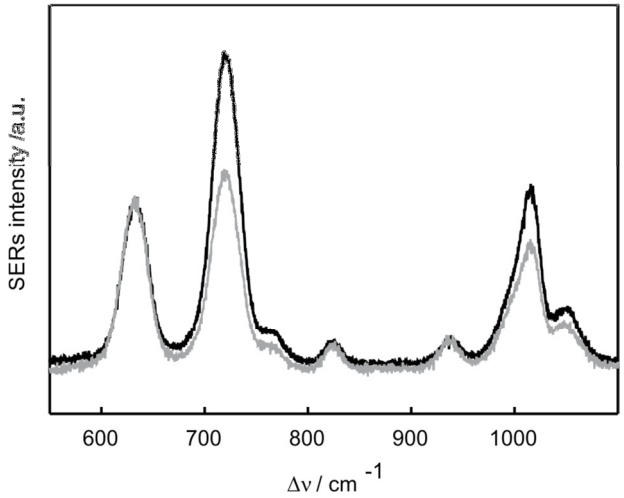

Figure SI 3. Effect of potential cycling on SER spectra. SER spectrum of OH-C2 before (grey) and after (black) 100 cycles between -0.2 and 0.15V at $0.1Vs^{-1}$.

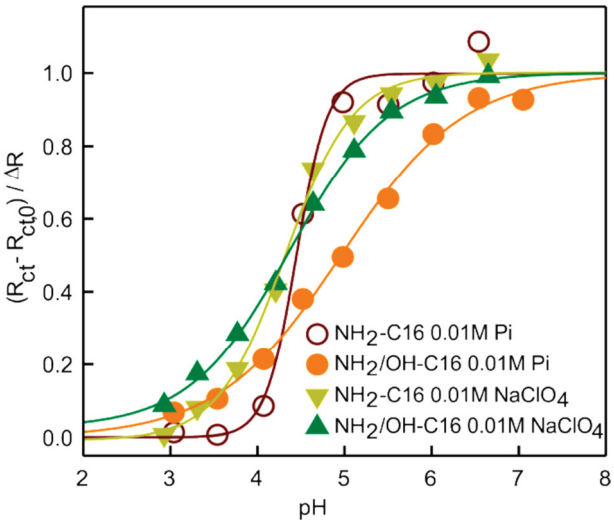

Figure SI 4. Normalized charge transfer resistance as a function of solution pH for NH_2 (0.01M Pi full circles, 0.01M $NaClO_4$ down triangles) and NH_2/OH-C16 electrodes (0.01M Pi empty circles, 0.01M $NaClO_4$ up triangles). Each point is the average of two electrodes. Lines correspond to the sigmoidal fit to eq. (8).

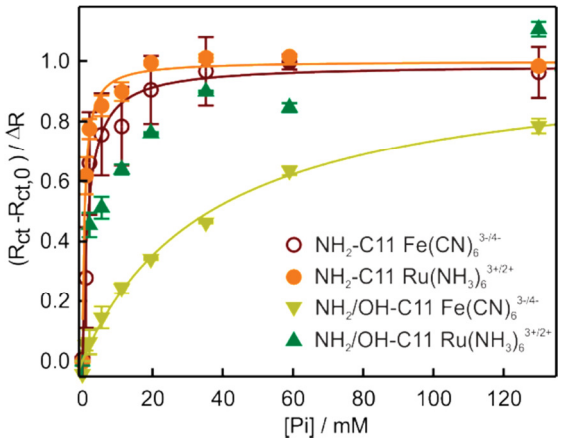

Figure SI 5. Normalized charge transfer resistance in the presence of two redox probes as a function of the Pi bulk concentration. $Fe(CN)_6^{-3/-4}$ on NH_2-C11 (empty circles) and NH_2/OH-C11 (down triangles) ; $Ru(NH_3)_6^{3+/2+}$ on NH_2-C11 (full circles) and NH_2/OH-C11 (up triangles).

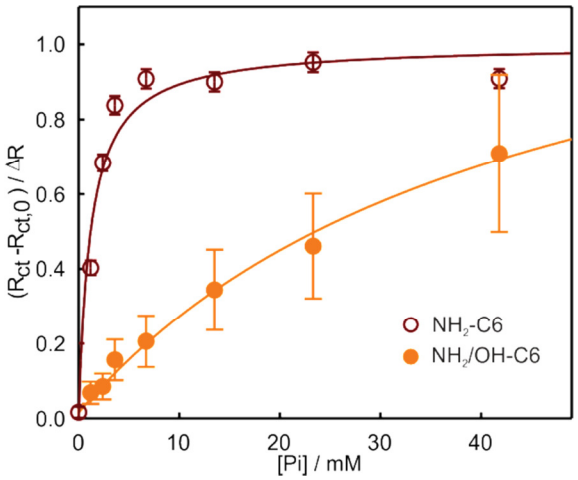

Figure SI 6. Normalized charge transfer resistance in the presence of $Fe(CN)_6^{3-/4-}$ probe as a function of the Pi bulk concentration; on NH_2 (full circle) and NH_2/OH-C6 (empty circles).

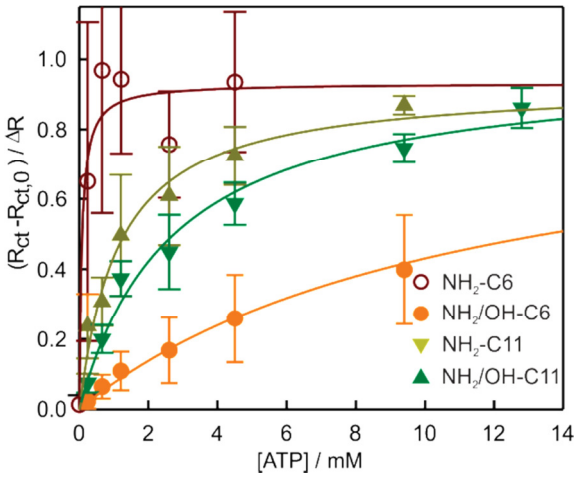

Figure SI 7. Normalized charge transfer resistance in the presence of $Fe(CN)_6^{3-/4-}$ probe as a function of the ATP bulk concentration; on NH_2-C6 (empty circles), NH_2/OH-C6 (full circles) NH_2-C11 (up triangles), and NH_2/OH-C11 (down triangles).

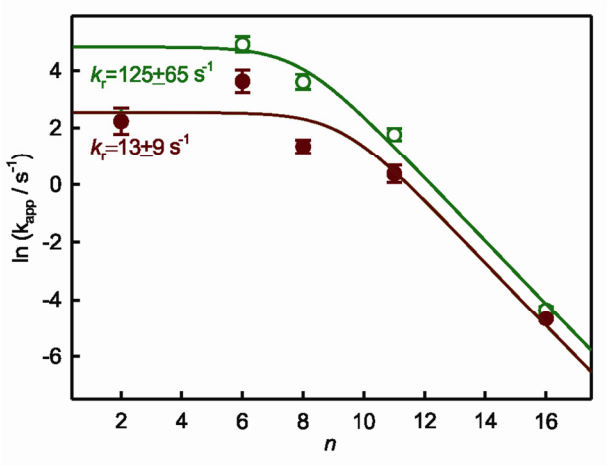

Figure SI 9. Apparent ET of Cyt *c* on NH_2 (full circle) and NH_2/OH-SAMs (empty circles) at zero overpotential in 0.01M Pi pH=7. Data for NH_2/OH-SAMs were determined by CV on gold electrodes while data for NH_2-SAMs were obtained by TR-SERRs measurements on silver electrodes. Bars indicate standard deviation (N=3). Lines correspond to fits to $k_{app}^{-1} = k_0^{-1}\exp(\beta n) + k_r^{-1}$, with $\beta = 1.1$.

REFERENCES

(1) Cao, X.-W. Study of electrode potential effect on acid–base behavior of ω-functionalized self-assembled monolayers using fourier transform surface-enhanced raman scattering spectroscopy. *J Raman Spectrosc* **2005**, *36*, 250–256.

(2) Nishiyama, K.; Kubo, A.; Ueda, A.; Taniguchi, I. Surface pka of amine-terminated self-assembled monolayers evaluated by direct observation of counter anion by ft-surface enhanced raman spectroscopy. *Chem Lett* **2002**, *31*, 80–81.

(3) Vegte, E. W. Van Der; Hadziioannou, G. Acid-base properties and the chemical imaging of surface-bound functional groups studied with scanning force microscopy. *J Phys Chem B* **1997**, *101*, 9563–9569.

(4) Scavetta, E.; Solito, A. G.; Demelas, M.; Cosseddu, P.; Bonfiglio, A. Electrochemical characterization of self assembled monolayers on flexible electrodes. *Electrochim Acta* **2012**, *65*, 159–164.

(5) Molinero, V.; Calvo, E. J. Electrostatic interactions at self assembled molecular films of charged thiols on gold. *J Electroanal Chem* **1998**, *445*, 17–25.

(6) Munakata, H.; Oyamatsu, D.; Kuwabata, S. Effects of omega-functional groups on ph-dependent reductive desorption of alkanethiol self-assembled monolayers. *Langmuir* **2004**, *20*, 10123–8.

(7) Wallwork, M. L.; Smith, D. A.; Zhang, J.; Kirkham, J.; Robinson, C. Complex chemical force titration behavior of amine-terminated self-assembled monolayers. *Langmuir* **2001**, *17*, 1126–1131.

(8) Vezenov, D. V.; Noy, A.; Rozsnyai, L. F.; Lieber, C. M. Force titrations and ionization state sensitive imaging of functional groups in aqueous solutions by chemical force microscopy. *J Am Chem Soc* **1997**, *119*, 2006–2015.

(9) Chatelier, R. C.; Drummond, C. J.; Chan, D. Y. C.; Vasic, Z. R.; Gengenbach, T. R.; Griesser, H. J. Theory of contact angles and the free energy of formation of ionizable surfaces: application to heptylamine radio-frequency plasma-deposited films. *Langmuir* **1995**, *11*, 4122–4128.

(10) Fears, K. P.; Creager, S. E.; Latour, R. A. Determination of the surface pk of carboxylic- and amine-terminated alkanethiols using plasmon resonance spectroscopy. *Langmuir* **2008**, *24*, 837–843.

(11) Degefa, T. H.; Schön, P.; Bongard, D.; Walder, L. Elucidation of the electron transfer mechanism of marker ions at sams with charged head groups. *J Electroanal Chem* **2004**, *574*, 49–62.

(12) Schweiss, R.; Werner, C.; Knoll, W. Impedance spectroscopy studies of interfacial acid-base reactions of self-assembled monolayers. *J Electroanal Chem* **2003**, *540*, 145–151.